Karazin Kharkiv National University
Faculty of Physics and Technology
Experimental Nuclear Physics Department

Deutsches Elektronen-Synchrotron
Photo Injector Test Facility in Zeuthen

Transverse Beam Size Measurement Systems at Photo Injector Test Facility in Zeuthen

Master's Thesis

by Roman Spesyvtsev

Supervised by
M. Sc. Lazar Staykov
Dr. rer. nat. Sergiy Khodyachykh

Zeuthen 2007

Abstract

The Photo Injector Test facility in Zeuthen (PITZ) at DESY is used to develop and characterize electron sources which produce a nominal bunch charge of 1 nC with the lowest possible transverse emittance. Beam size measurements provide us with knowledge on important beam characteristics. For example the measurement of the emittance is based on beam size measurements. Therefore, the control of uncertainties of beam size measurements is very important to validate the experimental results.

Three beam size measurement techniques are used at PITZ: scintillation screen stations (YAG), optical transition radiation (OTR) screen stations and wire scanners. The YAG screen stations are the most widely used devices because of their high sensitivity at low beam energy (5 - 13 MeV). On the other hand the OTR screens have better spatial resolution and can be used at higher electron beam energies. The wire scanners have no optics that exclude some systematical uncertainties but they have low speed of measurement and are sensitive to beam losses. Theoretical and experimental comparisons between the beam size measurement methods used at PITZ are presented in the thesis.

Анотація

Стенд випробувань фотоінжекторів PITZ використовується для розробки та вивчення характеристик джерел електронів, що випромінюють пучки з номінальним зарядом в 1 нКл та якомога меншим емітансом. Одним з базових вимірювань є вимірювання поперечного розміру електронного пучка. Наприклад вимірювання емітансу базується на вимірюваннях розміру пучка. Таким чином врахування невизначеності вимірів розміру пучка є важливим для визначення вірогідності експериментальних результатів.

У роботі представлені три методи вимірювання поперечного розміру електронного пучка, що використовуються в PITZ: сцинтиляційний екран (YAG), екран перехідного випромінювання (OTR) та дротяний сканер. YAG екрани найбільш поширені у PITZ завдяки їх високій чутливості до низькоенергетичних електронів (5 - 13 МеВ). З другого боку, OTR екрани мають краще просторове розрізнення і можуть використовуватися за умов більш високих енергій. Дротяні сканери не мають оптики, що виключає деякі систематичні похибки вимірювань, але вони мають низьку швидкість вимірювання та чутливі до втрат пучка. У цій роботі проведені теоретичне та експериментальне порівняння методів вимірювання поперечного розміру електронного пучка, що використовуються у PITZ.

Аннотация

Стенд испытания фотоинжекторов PITZ используется для разработки и изучения характеристик источников электронов, которые способны производить пучки с номинальным зарядом в 1 нКл и малым поперечным эмитансом. Одним из базисных измерений при характеризации источника электронов является измерение поперечного размера электронного пучка. В частности, измерение поперечного эмитанса основано на измерениях размера пучка. Знание погрешности в измерении размера пучка является очень важным условием для определения достоверности экспериментальных результатов.

В работе представлены три метода измерения поперечного размера электронного пучка, которые используются в PITZ: сцинтилляционный (YAG) экран, экран переходного излучении (OTR) и проволочный сканер. Наиболее используемой установкой в PITZ является YAG экран благодаря его хорошей чувствительности к низко энергетическим электронам (5 - 13 МэВ). С другой стороны, OTR экран имеет лучшее разрешение и может применяться при более высоких энергиях пучка. В работе проведено теоретическое и экспериментальное сравнение методов измерения поперечного размера электронного пучка в PITZ.

Contents

1 Introduction

Moving electrons with an acceleration perpendicular to their velocity radiate electromagnetic radiation. Using a periodical magnet structure (undulator) it is possible to produce coherent electromagnetic radiation. Such radiation sources are called Free Electron Laser (FEL). The main goal is to reach low wavelength radiation with a high brilliance. It requires a high quality electron beam source [2]. The Photo Injector Test facility in Zeuthen (PITZ) should provide the European XFEL project with such an electron source [3].

An important beam quality parameter is the transversal emittance that characterizes a beam in the transversal plane of the coordinate and the divergence (x, x'). The normalized RMS emittance can be expressed as [4]:

$$\epsilon = \gamma\beta\sqrt{\langle x^2\rangle \langle x'^2\rangle - \langle xx'\rangle^2} \tag{1}$$

where $\sqrt{\langle x^2\rangle}$ is the beam RMS size, $\sqrt{\langle x'^2\rangle}$ is the beam RMS divergence, $\langle xx'\rangle^2$ is the correlation term, γ and β are the mean energy and velocity of the bunch, respectively.

There are many experimental techniques available for transverse emittance measurements, namely: slit methods, quadrupole scan, tomography reconstruction etc. Most of these techniques use transverse beam size measurements for emittance calculations. Therefore, the beam size measurement techniques and uncertainty in their measurements are very important for electron sources characterization.

Three types of diagnostic tools for beam size measurements are implemented at PITZ: Yttrium Aluminum Garnet (YAG) multi-crystal screens, optical transition radiation (OTR) screens and wire scanners. In this work the electron beam size diagnostic systems are discussed.

Section 2 describes shortly the PITZ setup including a drive-laser, accelerating modules and diagnostics. In Section 3 an overview of beam size diagnostics at PITZ is given with some theoretical discussions. Separately, the optical system and camera setup are described in this section as an important part of the YAG and the OTR stations.

In Section 4 the experimental and simulation studies of the beam size diagnostic systems are shown. Comparative measurements between different systems were made. The beam dynamic influence on beam size measurements was studied. Cameras and signal transmission are also investigated systematically as an important part of the YAG and OTR screen stations. The systematical uncertainties of the YAG screen station are estimated. ASTRA scientific software [5] was used for beam dynamic simulations and GEANT4 [6] for the investigation of the interaction between the particles and detector components.

2 Photo injector setup

The main goal of the PITZ project is to develop and characterize electron sources which produce bunches with a nominal charge of 1 nC, low transverse emittance and short pulse length which are necessary to fulfill the requirements of the European XFEL project [2]. An ultra violet drive-laser is used to produce electron bunches and control their formation. The laser beam has a periodical time structure. Laser pulses having a length of about 20 ps form trains with duration of up to 900 μs. The distance between pulses in the train is 1 μs. The trains are produced with a repetition rate of up to 10 Hz. The transversal and longitudinal profiles of a laser pulse can be adjusted to reach the minimum beam transverse emittance of the electron beam. The main laser parameter are listed in Table 1. Laser beam diagnostics at PITZ is described in [7].

Table 1: Main laser parameters.

Main laser parameters	
Wavelength	262 nm
Pulse energy on the cathode	5 μJ
Repetition rate	5 Hz
Train length	1 $\div$ 900 μs
Pulse length	20 ps

The PITZ setup with acceleration modules and diagnostic systems is shown schematically in Fig. 1. Cs_2Te with a Mo sublayer is used as a photocathode [8]. The cathode emits electrons when illuminated by a laser beam. A 1.5 cell cavity accelerates the emitted electrons to about 5 MeV/c. The peak electric field in the cavity can reach 44 MV/m. The

main solenoid is used for compensating the space charge emittance growth. The solenoid magnetic field on the axis is given by equation B_z [T] $\cong$ $5.9 \cdot 10^{-4} I_{main}$ [A] $+3.6 \cdot 10^{-4}$ where the maximum value of the solenoid current is 500 A. The bucking solenoid is necessary for compensation of the magnetic field on the photocathode surface which is induced from the main solenoid. The booster is situated at 3 m downstream from the cathode. It has about 15 MV/m peak electric field and accelerates the electrons up to 13 MeV/c. The gun and the booster are supplied from 10 MW and 5 MW klystrons (1.3 GHz). The whole setup can be divided into two parts - the low energy section before the booster and the high energy section after the booster.

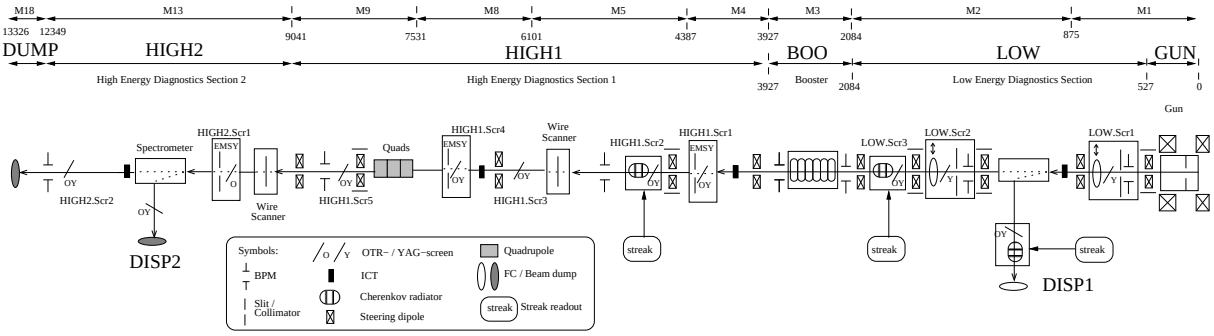

Figure 1: PITZ setup scheme. Summer 2006.

The high energy section has one additional quadrupole triplet that focuses the beam after the booster. There are ten steering magnets to correct the orbit of the electron beam along the beam pipe. Beam position monitors are mounted along the beam pipe to control the orbit of the beam.

For charge measurements integrating current transformer (ICT) monitors [9] are used in both the low and the high energy sections. When the electron bunch passes through the ICT a voltage is induced which is linearly proportional to the bunch charge. An ICT measures the bunch charge without beam destruction but it is not sensitive to bunch charge

below 100 pC at PITZ. The Faraday cups (FCs) [9] are used for charge measurements in the low energetic section. A FC collects electrons and transmits the signal to the oscilloscope afterward. Ten screen stations are installed for the beam profile measurements. Three of the stations are the Emittance Measurement SYstems (EMSYs) which are equipped with a Tungsten slit masks and OTR and YAG screens for the emittance measurements [10]. Also two wire scanners were mounted and tested as an alternative device for the transversal beam profile measurements [11]. Other important diagnostic elements are two electron spectrometers. They bend the trajectory of the electrons in a magnetic field by 60 deg. The bend angle is proportional to the magnetic field. One can measure the mean beam momentum and momentum spread after the gun in the low energy dispersive arm (LEDA) and after the booster in the high energy dispersive arm (HEDA) [12]. They contain also screen stations.

3 Electron beam size measurements

The measurement of a beam size is one of the basic measurements for the characterization of an electron beam. One of the most important beam characteristics is the transverse beam emittance, which is proportional to the volume that electrons occupy in the phase space ($\vec{r}$, $\vec{p}$) [13], where $\vec{r}$ and $\vec{p}$ are the space and the momentum vectors respectively. Most of the methods for emittance determination are based on beam size measurements. The main method for the emittance measurements used in PITZ is the slit method. During the last operating period EMSY stations were implemented and used for transverse emittance measurements at PITZ [14]. The method uses the beam and beamlet RMS size measurements to calculate the emittance. A beamlet is a part of a beam that is cut with a slit mask. The beam RMS size is measured at the EMSY position with a YAG screen. For a beam divergence calculation one uses the 10 μm or 50 μm slit at the EMSY position to scan the beamlet RMS size along the beam profile. The beamlet profile is measured in two meters after the EMSY station. Typical values of a beam RMS size is 0.5 mm and a beamlet RMS size about 0.2 mm but a beamlet RMS size can amount to values down to 40 μm [15].

Quadrupole scan and multi screen methods are two additional alternative methods for emittance measurements. Moreover, using tomography technique, one can reconstruct phase space distribution of the beam. The tomography reconstruction also uses beam size measurements. The tomography module is under design for the next stage of the PITZ setup [16].

3.1 Scintillation screen

The most usable beam size monitor at PITZ is the scintillation screen. The reason is that the scintillator has higher sensitivity to low energy electron beam (5 ÷ 13 MeV) than OTR screen. The Ce-doped Yttrium Aluminum Garnet (YAG) multi-crystal material is used at PITZ as an scintillator. It is a radiation stable material and has good mechanical and vacuum properties, is chemically inert and not hygroscopic. It is possible to use either solid YAG crystal (with a 250 ÷ 500 μm thickness) or the small layer of YAG powder (down to 5 μm) on a substrate material (for example Si). There is only the second type of a YAG screen in use at PITZ. The main properties of the YAG screen used at PITZ are listed in Table 2.

Table 2: YAG:Ce screen properties.

YAG:Ce screen properties	
Chemical formula	$Y_3Al_{2,5}Ga_{2,5}O_{12} : Ce$
Index of Refraction	1.82
Wavelength of peak emission	510 nm
Density of the scintillator material	5.1 g/cm^3
Scintillation efficiency (compare to NaI)	45%
Thickness of scintillator layer	between 5μm and 20μm
Thickness of Silicon sublayer	0.275 mm
Density of Silicon	2.33 g/cm^3

The light output from a YAG crystal is proportional to the energy deposition in it for the energy range above the energy excitation threshold and below the range of saturation. The energy deposition in the YAG layer

versus electron energy is shown in Fig. 2. High energy secondary particles escape from the crystal medium without significant energy deposition in it. Therefore the energy deposition in the crystal is less than the losses of the primary particle. After the beam passes through the screen the light output profile should repeat the electron beam distribution but in the reality it differs from the original electron beam distribution due to the multiple scattering (see Section 4.2), saturation at higher charge densities and optics effects (see Section 3.4).

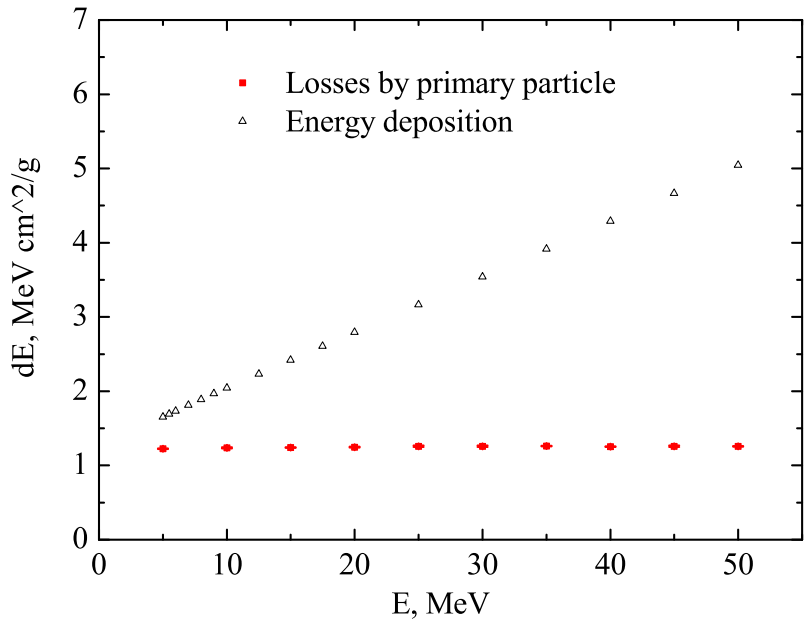

Figure 2: Energy deposition in the YAG layer. Energy losses by primary electron were taken from [17] and the energy deposition was simulated using GEANT4.

Part of the energy deposited in the medium excites the f-level of donor atoms (Ce) which illuminate light afterwards [18]. The reason that leads to a YAG screen saturation is the limited amount of the light-emitting centers (Ce atoms). The medium excitation in the scintillator is described

by the differential equation [19]:

$$\frac{dn_{ph}}{dn_{eh}} = q\beta\left(1 - \frac{n_{ph}}{qN}\right), \tag{2}$$

where n_{eh} is the density of electron-hole pairs generated, n_{ph} is a density of photons emitted, q and β - quantum and transport efficiency respectively, N is a density of Ce atoms. The solution of Eq. (2) gives the relationship between the actual beam profile $\Sigma(r)$ and the measured beam profile $\Sigma_Y(r)$ [19]:

$$\Sigma_Y(r) = \frac{1 - e^{-\alpha\Sigma(r)}}{\alpha}, \tag{3}$$

$$\alpha = \frac{\beta}{eN} N_{eh} \frac{dE}{dx}, \tag{4}$$

where α is the saturation constant (α^{-1} is an upper limit of the charge intensity that one can observe with a YAG screen), $q = 1$, N_{eh} the number of $e - h$ pair production per one MeV of the deposited energy, dE/dx the energy deposition in the medium, e is the charge of electron. To estimate the saturation constant supposed that $\beta = 1$, the concentration of Ce atoms is known $N = 2.5 \cdot 10^{-19}$ cm^{-3}, $N_{eh} = 60000$ MeV^{-1} [19], the energy deposition by primary electrons with 13 MeV initial energy is 10 MeV/cm, thus:

$$\alpha^{-1} = 66.6 fC/\mu m^2. \tag{5}$$

Let us try to estimate an influence of the saturation effect on a measured beam RMS size. As an initial beam distribution we take a sum of two Gauss functions:

$$g(r) = \frac{Q_1}{2\pi\sigma_1^2} e^{-\frac{r^2}{2\sigma_1^2}} + \frac{Q_2}{2\pi\sigma_2^2} e^{-\frac{r^2}{2\sigma_2^2}}. \tag{6}$$

The first Gauss function corresponds to the beam core and the second one describes the beam halo. The full charge Q and the RMS size σ of the

distribution are:

$$Q = Q_1 + Q_2, \qquad \sigma^2 = \frac{2(Q_1\sigma_1^2 + Q_2\sigma_2^2)}{Q_1 + Q_2}. \tag{7}$$

The light output from the YAG screen $g_Y(r)$ is determined by Eq. (3)

$$g_Y(r) = \frac{1 - e^{-\alpha g(r)}}{\alpha}, \tag{8}$$

and the corresponding RMS size is

$$\sigma_Y^2 = \frac{\int g_Y(r) r^2 d^2 r}{\int g_Y(r) d^2 r}. \tag{9}$$

In the theoretical calculations we varied two parameters to change the initial distribution $g(r)$:

$$k = \frac{Q_1}{Q} \quad \xi = \frac{\sigma_1}{\sigma_2}. \tag{10}$$

The total bunch charge $Q = 1$ nC corresponds to the usual operating regime at PITZ. The RMS size of the initial distribution $\sigma = 0.3$ mm. Results of the theoretical calculations are shown in Table 3.

Table 3: Theoretical estimation of the YAG screen saturation effect.

k		ξ			
		0.1	0.3	0.5	0.7
0.8	g(0), fC/μm^2	59	8.7	4.8	3.8
	σ_Y, mm	0.324	0.303	0.302	0.301
0.6	g(0), fC/μm^2	86.7	11.4	5.5	4
	σ_Y, mm	0.327	0.304	0.302	0.301

From Table 3 one can calculate the difference between the initial RMS size σ and RMS size of the light distribution σ_Y. The difference depends on the peak charge density and can reach about 1% at charge density of

10 fC/μm^2 and 8% at charge density of 60 fC/μm^2. The real value of the saturation parameter α can differ from the theoretical estimations. To know the systematical uncertainty of the effect one has to find this parameter experimentally. The experimental measurements of the saturation effect were done for 5 MeV electron beam in [20] and for 100 MeV electron beam in [19]. In the Section 4.1 the experimental study was done for 13 MeV electron beam.

The light is not illuminated immediately but during a finite time and it is a statistical process. Therefore another important characteristic of the scintillator is the decay time constant, τ. This is the time after which the number of the excited light-emitting centers decreased by factor of e. There are two decay time constants for the YAG crystal because of two different ways of the light-emitting centers excitation. The first and the second decay time constants for the YAG scintillator are $\tau_1 \sim 105$ ns and $\tau_2 \sim 487$ ns respectively [21]. Both of them are less than the distance between the bunches in the train (1 μs). Therefore the YAG screen separates the bunches in time. In case the time between bunches is less than $\tau_{1,2}$ the saturation effect would have a bigger influence. This can happen at PITZ if the time between pulses is decreased down to 0.5 μs.

3.2 OTR screen

When a particle crosses the boundary between two media with a different index of refraction a resultant radiation appears. This radiation is called transition radiation. The intensity and the angle distribution of the OTR are calculated from the Maxwell equations [22]. The simple scheme of the OTR screen station is shown in Fig. 3. The electron beam inter-

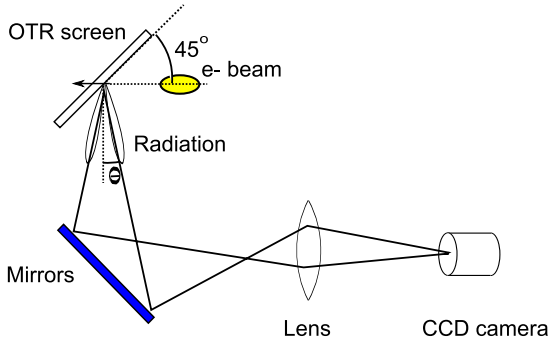

Figure 3: Scheme of the OTR screen station.

acts with a metal OTR screen placed under 45 deg angle to the beam axis. The produced light is focused by an optical system and collected by a CCD camera. For our simple geometry and for the boundary conditions vacuum-metal the transition radiation intensity is given by [22]

$$\frac{d^2I}{d\omega d\Omega} = \frac{e^2}{\pi^2 c}\frac{\sin^2\theta}{(\gamma^{-2}\cos^2\theta + \sin^2\theta)^2}, \tag{11}$$

where e is the electron charge and ω is the radiation frequency. The intensity depends on the particle energy $E = \gamma mc^2$ and on the observation angle θ. In case of small observation angles ($\theta << 1$) equation (11) becomes

$$\frac{d^2I}{d\omega d\theta} = \frac{2e^2}{\pi c}\frac{\theta^3}{(\gamma^{-2} + \theta^2)^2}, \tag{12}$$

where we have used the relationship $d\Omega = 2\pi \sin\theta d\theta$. The emission angle of the OTR radiation depends on the particle energy

$$\theta = \frac{1}{\gamma}, \tag{13}$$

which corresponds to the maximum intensity in Eq. (12) (see Fig. 4 (left)).

In case the focus plane of our optical system approaches to infinity one can observe an angular dependence of the signal intensity (see Fig. 4 (left)). The curve has two peaks at two symmetric points $\theta = \pm\gamma^{-1}$. At low energetic beam the peaks are far from the center and the light distribution

becomes wider. Therefore, only a small part of the light passes through the optical aperture. For the electron beam with a divergence distribution $f(\theta')$ the angular dependence is a convolution of Eq. (11) and $f(\theta')$:

$$\frac{d^2W(\theta,\gamma)}{d\omega d\Omega} = \int \frac{d^2I}{d\omega d\Omega}(|\theta-\theta'|)f(\theta')d\theta', \tag{14}$$

where θ is the observation angle. The angular dependence can be used for the beam energy determination as well as for the divergence determination [23].

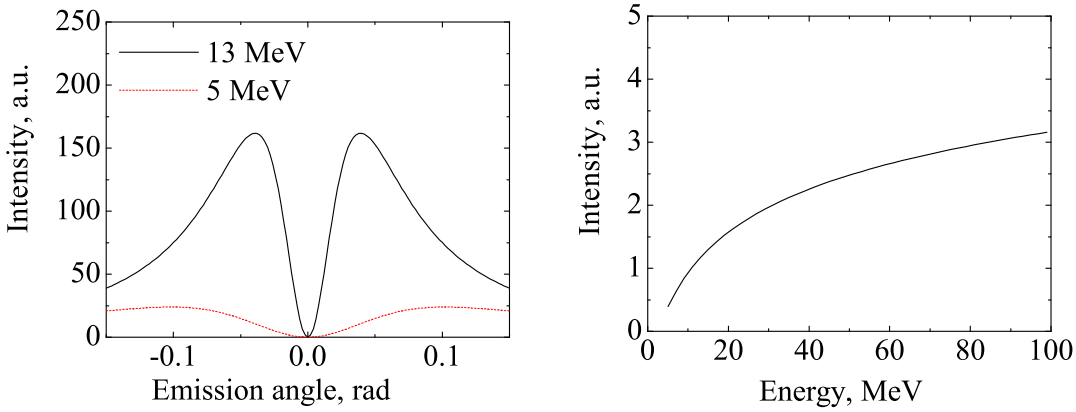

Figure 4: OTR intensity versus emission angle for 5 MeV and 13 MeV electron beam (left) and versus energy for the optical aperture $\theta_m = 0.2$ rad (right).

If we focus our optical system on an OTR screen plane we can measure the electron beam profile. The whole intensity of the light for the optical aperture $\theta_m = 0.2\ rad$ (the optical aperture for the PITZ screen stations) can be calculated from Eq. (12):

$$I = \int_0^{\theta_m} \frac{2e^2}{\pi c}\frac{\theta^3}{(\gamma^{-2}+\theta^2)^2}d\theta. \tag{15}$$

The integral (15) can be taken analytically:

$$I = \ln(1 + \gamma^2\theta_m^2) + \frac{1}{1 + \gamma^2\theta_m^2}. \tag{16}$$

This dependence is a logarithmic function of the particle energy (see Fig. 4 (right)). The experience at PITZ shows that the light output from an OTR screen is not enough for beam size measurements at 5 MeV electron beam energies. At 13 MeV electron beam OTR gives a reasonable light output but it is still by a factor of eight less than for a YAG screen.

3.3 Wire scanner

Wire scanners are widely used for beam profile measurements in acceleration physics. The principle of the measurement is based on the bremsstrahlung losses and the production of secondary electrons by the primary beam in the wire material (Fig. 5). The secondary electrons and γ rays deposit energy in a scintillator which is situated out of the beam pipe. The light from the scintillator is collected by optical fibers and is detected by a photomultiplier. After the signal intensity is measured for different positions of the wire the given distribution will correspond to the electron beam profile. The beam losses on the vacuum system components are detected by the scintillator as well as the signal from the wire. Therefore one has to minimize beam losses to decrease the noise level.

The wire scanner at PITZ has two wires for both X and Y planes. The spacing between wires is 10 mm. The material of the wires can be tungsten or carbon 10 μm in diameter (in general diameter can be varied from 5 to 80 μm) [25]. Wires can be moved with a speed range v = 0.1 $\div$ 1000 mm/s. To scan l = 1 mm of the beam with the wire scanner it takes minimum t = 1 ms. Thus, the beam position jitter influences wire scanner measure-

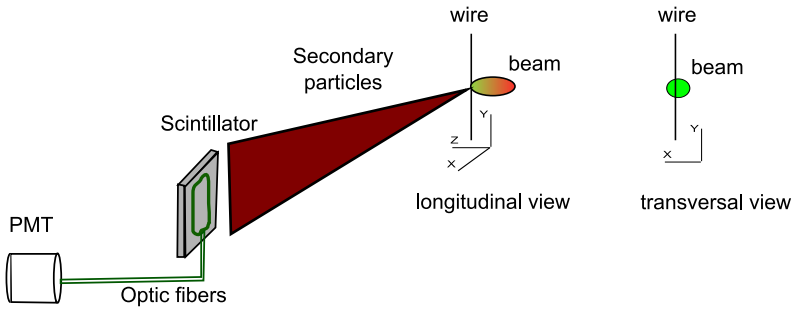

Figure 5: Scheme of the wire scanner work.

ments to bigger extend than for other methods because the measurement for each wire position corresponds to different trains. Because of the mechanical properties only one axis can be scanned at the same time.

The additional uncertainty due to the finite thickness of the wire is given by equation [26]

$$\sigma_{meas} = \sqrt{\sigma_{real}^2 + \left(\frac{d_{wire}}{4}\right)^2}, \tag{17}$$

where σ_{meas} is the measured beam RMS size, d_{wire} is the wire diameter and σ_{real} is the real beam RMS size for the Gaussian distribution.

The bremsstrahlung cross section and secondary electrons production are very sensitive to the beam energy. A wire scanner has low intense signal for a low energy electron beam. The signal intensity from the wire grows up with increasing beam energy. Wire scanners were installed at PITZ and tested for 5 MeV [11] and for 13 MeV electron beam energies. The measurements showed good resolution for both beam energies. The comparison measurements between the wire scanner and the YAG screen stations are done in Section 4.3.1.

3.4 Optical system

The light from YAG or OTR screens is collected and focused with the optical system to the camera CCD chip. After any optical system the image of a point light source is a light distribution with a finite size. Let us describe a one-dimensional image of a point light source by a Gauss function:

$$g(x) = \frac{1}{\sqrt{2\pi}s} e^{-\frac{x^2}{2s^2}} \tag{18}$$

To find the relationship between the parameter s and the optical resolution we use the definition of the modulation transfer function (MTF)

$$z(\omega) = \int_{-\infty}^{\infty} g(x) e^{-i\omega x} dx, \tag{19}$$

where ω is called spatial frequency. The optical resolution ω_0 is often determined as a solution of the Eq. (19):

$$z(\omega_0) = 0.1 \tag{20}$$

The unit of measurement of the resolution ω_0 is mm^{-1}.

A degraded beam image distribution $f_{deg}(x)$ after the optical system can be found from the convolution of the point spread function (18) with the initial distribution $f(x)$:

$$f_{deg}(x) = \int_{-\infty}^{\infty} f(y-x) g(y) dy. \tag{21}$$

A sum of two Gauss functions is taken as an initial light distribution (see Section 3.1):

$$f(x) = \frac{Q_1}{\sqrt{2\pi}\sigma_1} e^{-\frac{x^2}{2\sigma_1^2}} + \frac{Q_2}{\sqrt{2\pi}\sigma_2} e^{-\frac{x^2}{2\sigma_2^2}}, \tag{22}$$

The beam RMS sizes are determined for the distributions $f(x)$ and $f_{deg}(x)$:

$$\sigma = \frac{\int f(x) x^2 dx}{\int f(x) dx}, \qquad \sigma_{deg} = \frac{\int f_{deg}(x) x^2 dx}{\int f_{deg}(x) dx}, \tag{23}$$

respectively. Using Eq. (21) one can estimate the influence of the optical resolution on the beam RMS size measurements. The difference $\delta\sigma = \sigma_{deg} - \sigma$ between the RMS sizes of the functions $f_{deg}(x)$ and $f(x)$ related to the initial beam size is shown in Fig. 6 as a function of optical resolution ω_0 (see Eq. (23)). This difference does not have visible dependence from the initial beam profile.

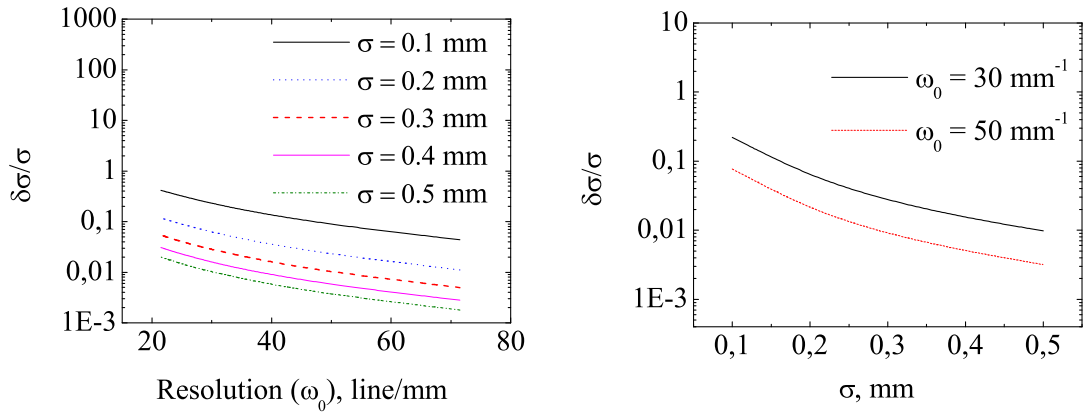

Figure 6: Influence of the optical resolution on the measured beam RMS size.

The PITZ facility uses the lens type "Optem Macro video zoom" produced by the company "Qioptiq Imaging Solutions" [27]. The resolution of the optical system depends on the magnification and it is in the range of 20 $\text{mm}^{-1} \div 50\ \text{mm}^{-1}$. The higher the magnification of optical system is the better the resolution is.

Often the image of an object is not located in the image plane of the optical system. For example because of the finite thickness of the scintillator layer for YAG screen or because of the 45 degree angle between the screen and the focal plane for the OTR screen. Due to this the light from the point source is distributed in the image area with a radius $r = z \cdot \theta_{max}$ [28],

where z is the distance from the source to the focal plane and θ_{max} is the optical aperture. This effect increases the measured beam RMS size.

3.5 Camera and signal distribution

The camera and the signal transportation systems are important parts of the beam size measurements for screen stations. A simple description of the PITZ camera system is shown in Fig. 7. The light from the YAG screen is converted into charge located in the cells of a charge-coupled device (CCD chip). The charge in the CCD chip cells is readout and converted to

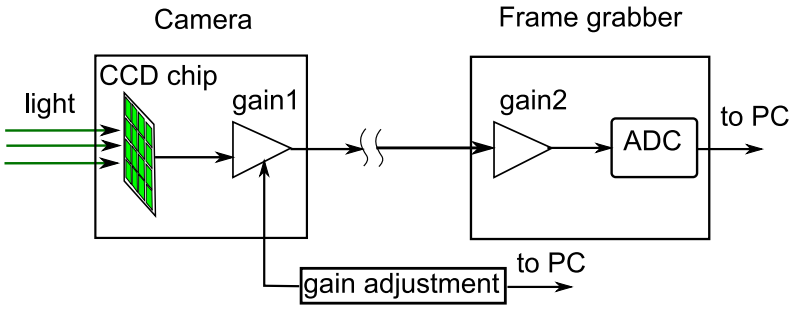

Figure 7: Simple scheme of the light detection.

an analog signal, amplified and transported to the frame grabber through a long cable (∼40÷60 m). The gain in the CCD camera (gain1) is software-adjustable during operation. The amplification range can be adjusted from 0 to 24 dB. The gain inside the frame grabber (gain2) is set to a constant defined value during the operation. In the frame grabber the analog signal is sampled and thus, converted to a digital one (at PITZ, 8-bit analog to digital converters (ADCs) are used). In ideal conditions an 8-bit ADC divides the signal intensity into 255 levels. JAI cameras [29] with a SONY CCD chip [30] are installed at PITZ.

The signal transformations can be divided into three steps:

1. Binning in CCD cells. A continuous spatial light distribution is converted into a discrete spatial distribution.

2. Signal readout from the CCD cells and transfer to the ADC. Signal attenuation and noise collection are possible during these processes.

3. Analog to digital conversion. After the ADC, signal values with an intensity that is less than the first ADC level are lost.

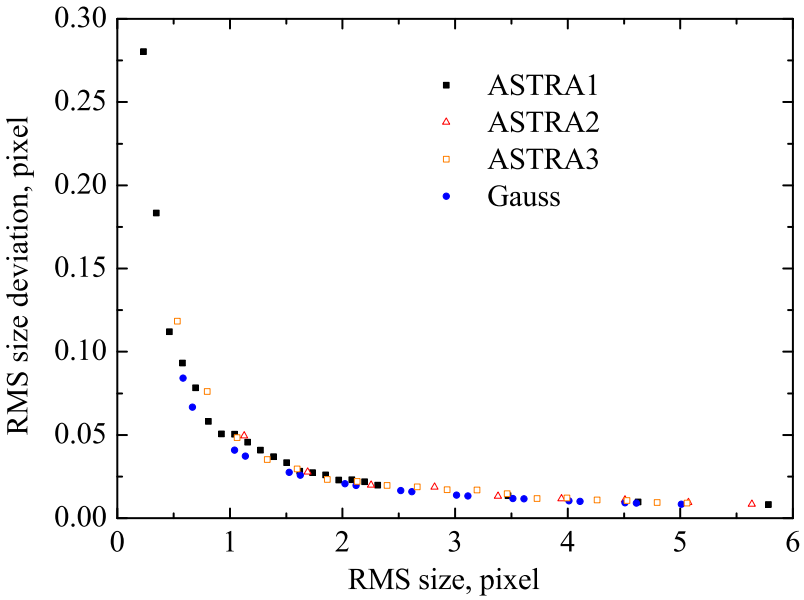

Figure 8: Difference between the RMS sizes for the continuous and discrete distributions. All sizes are shown in pixel unit. To transfer from pixel unit to millimeter the pixels must be multiplied by the real pixel size of the CCD chip and divided by the optical magnification.

After the binning in a CCD chip the RMS size of the discrete distribution differs from the original continuous one. The binning effect can be simulated numerically. For the accomplished simulations, the Gauss

function and several beam distributions, obtained from the ASTRA simulations which are close to the measurements at PITZ, were taken as initial distributions. The histogram was built for each distribution with variable transversal size of a pixel. The difference in the RMS sizes, as calculated by the simulations, between the continuous and discrete distributions is shown in Fig. 8. To estimate the influence of the binning in a CCD chip on beam size measurements the typical experimental parameters for the camera and optical system at PITZ were chosen. PITZ cameras have the pixel size of 8.3 μm (in x and y plane) and the minimum magnification used is 0.2. Therefore in worst case the pixel size in the image plane is about $8.3/0.2 \approx 40$ μm. The minimal expected beamlet RMS size is about 40 μm (1.0 pixels). Thus, the maximum deviation for the beam RMS size measurements at PITZ is 2 μm (0.05 pixel) (see Fig. 8). It is a systematical uncertainty in the measurements that increases the measured beam RMS size.

The theoretical estimation of the signal transportation behavior is not possible but some experimental investigations will be done in Section 4.5.

One of the main effect during the analog to digital conversion is the cutting of the distribution edges. This effect decreases the measured beam RMS size. For an 8-bit ADC the signal intensity that is less than $\frac{1}{256}$ from the peak intensity in the distribution can not be detected. A correct numerical estimation of the effect influence on the measurements is not possible for a general case because the behavior of the beam distribution can not be described by any simple function. One should simulate the beam profile with the ASTRA for each measurement to find out the systematical uncertainty [15].

Another important characteristic is the noise level of the camera. In

case the noise fluctuations are significantly larger than the first ADC level, the analog to digital conversion does not play any role. The edges of the image distribution will be lost in the noise fluctuations.

3.6 Summary

Three main techniques for the beam size measurements were described in this section, namely a YAG screen, an OTR screen and a wire scanner. A YAG screen has better sensitivity to the low energy beam ($5 \div 13$ MeV) than others. The light output from a YAG screen does not have a significant dependence on the beam energy as for the OTR screen station and wire scanner, but a YAG screen station has more possible systematical uncertainties than other devices. Both screens the YAG and the OTR can resolve one electron bunch but the light registration using a CCD camera allows to distinguish only several bunches ($\sim$2 μs). The OTR signal carries more information about an electron beam like beam energy, beam divergence and temporal beam profile. The wire scanner has good sensitivity to the beam as a YAG screen but the speed of the scan does not allow to resolve bunches and even cover several trains. It can include additional systematical uncertainty in the beam size measurements due to the beam position jitter. The possible systematical uncertainties for each device were considered with some theoretical calculations. The binning effect gives the maximum uncertainty of $\sim$1 μm. The uncertainty at 30 mm^{-1} optical resolution is about 20μm for 0.1 mm initial RMS size of the beam. For other optical resolution values and initial sizes of the beam one can find the uncertainty values in Fig. 6. Both the types of the uncertainties are decreased when increasing the initial beam size.

4 Experimental and simulation results

4.1 YAG screen saturation study

Theoretical estimations (see Section 3.1) show that saturation can make a visible influence on beam RMS size measurements at charge densities higher than 10 fC/μm^2. The goal of the present study was to check whether the saturation of YAG:Ce screen at PITZ influences on beam RMS size measurements. There are two possibilities to increase charge density: 1) increase beam charge or 2) decrease beam RMS size. The first one is limited by the photocathode QE and by the laser intensity and spot size. The second one is limited by beam dynamics and can be realized by focusing the beam using a quadrupole triplet or solenoid. The experiment was carried out at the screen station High1.Scr5 placed directly after the quadrupole triplet (see Fig. 1) where one can use, both the first and the second possibility.

There are two ways to check the YAG screen saturation. The first one is based on the comparison of the beam profile measured on the YAG screen with that obtained from measurement on the OTR screen which has no saturation effect [19]. This method could not be applied since there was no OTR screen at the same screen station. Using the second one, one investigates the dependence of the beam distribution as a function of the electron beam charge. The main idea of the study is to find the saturation parameter α (see Section 3.1).

The electron beam was focused by the quadrupole triplet in the beginning of the experiment to reach the minimum beam size. The quadrupole triplet current was not changed during the experiment. The charge density was varied by changing the initial charge of the bunch keeping the other

Table 4: Main beam parameters during the experiment.

Main beam parameters	
Mean momentum	11.7 MeV/c
Bunch charge	0.7 - 2 nC
Beam RMS size	$\sim$ 0.2 mm
Maximum charge density	4 fC/μm^2

injector parameters constant (Table 4). The electron beam profile was measured as a function of the bunch charge. Signal intensity versus charge is shown in Fig. 9. The maximum reachable charge density was equal to 4 fC/μm^2 at the beam charge of 2 nC. This value is below the theoretical estimation of the charge densities (10 fC/μm^2) which can influence the electron beam image profile.

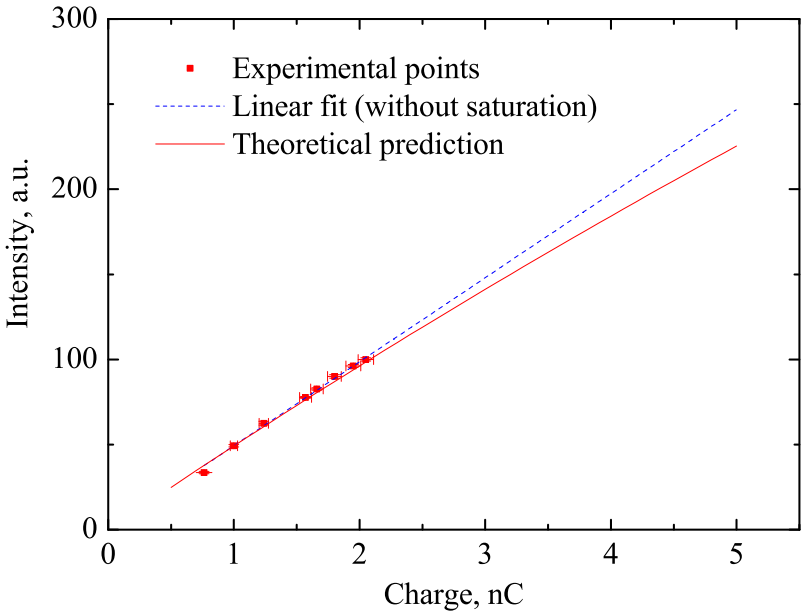

Figure 9: Signal intensity versus electron beam charge.

Detailed analysis of the experimental data was done to find the saturation parameter α in oder to compare it with the theoretical calculations (5). Let the original electron beam profile be $g(r)$ and the distribution of the

electron beam image after the YAG screen (distribution of the emitted photons) be $g_Y(r)$. The relationship between them is given by Eq. (3). The inverse conversion gives

$$g(r) = -\frac{1}{\alpha}\ln[1 - \alpha g_Y(r)b], \tag{24}$$

where b is the normalization constant. Integrating both sides of this equation, the left side gives full bunch charge Q

$$\int g(r)dr = Q, \tag{25}$$

and the right side gives a function with two parameters α and b

$$-\frac{1}{\alpha}\int \ln[1 - \alpha g_Y(r)b]dr = f(\alpha, b). \tag{26}$$

The charge Q and the distribution $g_Y(r)$ are measured in the experiment. According to the relationships (24), (25) and (26) the parameters α and b can be found from minimization

$$min \sum_{j=1}^{n}[Q_j - f_j(\alpha, b)]^2, \tag{27}$$

where n is the number of the experimental points ($n = 8$ in our case). Since the distribution $g_Y(r)$ is discrete, the integral (26) is represented as a sum

$$f(\alpha, b) = -\frac{1}{\alpha}\int \ln[1 - \alpha g_Y(r)b]dr = -\frac{1}{\alpha}\sum_i(\ln[1 - \alpha g_{Yi}b]\Delta r), \tag{28}$$

where Δr is the size of the camera pixel and g_{Yi} is proportional to the light density at pixel i. The maximum reachable charge density is less than the theoretical value $\alpha^{-1} = 66$ fC/μm^2. Therefore the product $\alpha g_Y(r)b$ is less than one and function $\ln[1 - \alpha g_{Yi}b]$ can be written as

$$\ln[1 - \alpha g_{Yi}b] = \sum_{k=0}^{\infty}\frac{(-1)^k}{k}(-\alpha g_{Yi}b)^k, \tag{29}$$

where the successive term is less than the previous one. Let us consider the first three terms from the series (29):

$$\begin{aligned} f(\alpha, b) &= -\frac{\Delta r}{\alpha}\sum_i(-\alpha g_{Yi}b - \frac{(\alpha g_{Yi}b)^2}{2} - \frac{(\alpha g_{Yi}b)^3}{3}) = \\ &= \Delta r(b\sum_i g_{Yi} + \alpha b^2\sum_i g_{Yi}^2 + \alpha^2 b^3\sum_i g_{Yi}^3) = \\ &= bf_0 + \alpha b^2 f_1 + \alpha^2 b^3 f_2 \end{aligned} \quad (30)$$

Using Eq. (27) we find the parameters α and b. The result of the minimization is $b = 0.01712$ and $\alpha = 0.013$. To validate the minimization we consider the numerical values of each term from Eq. (30) for the measurement with a charge $Q = 2$ nC (Table 5). Approximately the same order of magnitude the values are for the other experimental points.

Table 5: Numerical values of the terms from Eq. (30). All values are in nC.

Charge	Charge uncertainty	bf_0	$\alpha b^2 f_1$	$\alpha^2 b^3 f_2$
2.05	0.06	1.998	0.033	0.000864

The first and the second terms from the series are below the charge uncertainty. Therefore the saturation effect at 4 fC/μm^2 is above the uncertainty of the measurements and parameter α can not be validated in this experiment. To find the saturation parameter one has to increase charge density (to increase bunch charge) and to decrease the uncertainty in the measurements. The installation of both the screen types, the YAG and the OTR at the place of the maximum reachable charge density should be done to have an alternative method for the determination of the saturation parameter.

4.2 Multiple scattering in the YAG screen

In this section an image degradation due to the multiple scattering of the electrons is investigated. Passing through a matter primary electrons are scattered by the Coulomb potentials of nuclei and atom electrons. They create secondary electrons and photons and change the original direction of their movement. Due to these effects the image from a point source of electrons will be seen as a distribution with a finite RMS size and the beam profile measured with the YAG screen will differ from the original electron distribution.

For small scattering angles particles are normally distributed around average scattering angle $< \theta >= 0$. The root mean square of the projected scattering angle distribution is given by [31]

$$\sqrt{< \theta^2 >} = \frac{13.6 MeV/c}{\beta cp} z \sqrt{\frac{x}{X_0}} (1 + 0.038 \ln(\frac{x}{X_0})), \tag{31}$$

where p (in MeV/c) is the momentum, βc is the velocity and z is the charge of the scattered particle, and x/X_0 is the thickness of the scattering material, in units of the radiation length. Usual YAG screen at PITZ has thickness $x = 0.275$ mm of Silicon ($X_0 = 9.4$ cm). Mean electron momentum after the gun is about $p = 5$ MeV/c and after the booster is about $p = 15$ MeV/c. The RMS size of the image from a point electron source can be estimated as

$$\sigma = \sqrt{< \theta^2(p) >} \cdot x. \tag{32}$$

The estimations give 30 μm RMS size of the point electron source at $p =$ 5 MeV/c and 10.5 μm at $p = 15$ MeV/c. This effect increases an original beam RMS size.

Monte Carlo simulations were done to determine the influence of the

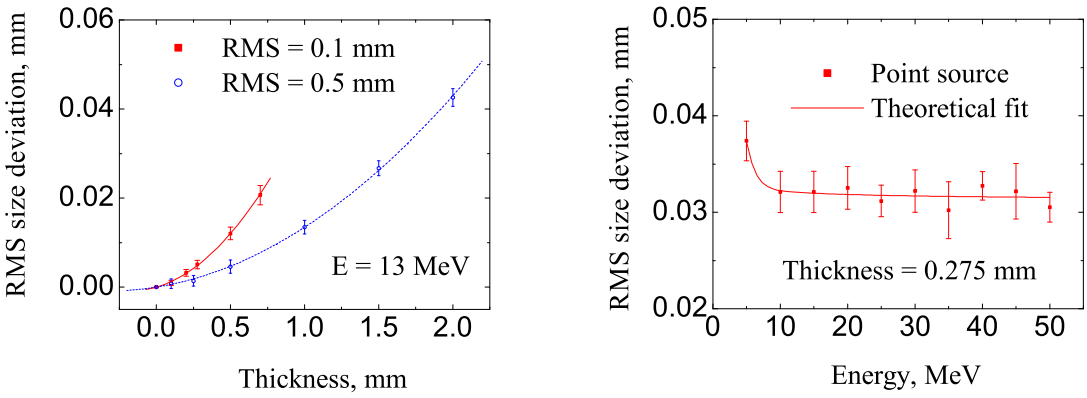

Figure 10: GEANT4 simulations of RMS size deviation due to the multiple scattering versus screen thickness (left) and electron energy (right). In the right graph electron energy is 13 MeV.

multiple scattering on the beam size measurements. GEANT4 was used for these simulations. The YAG screen properties which were used in the simulations are listed in Table 2. Gauss function was taken as an initial particle distribution. Simulations were done for two different initial RMS sizes of the beam of 0.1 mm and 0.5 mm. For each simulation 10^6 initial particles were generated. The signal from a YAG screen is proportional to the energy deposition in the screen. The deviation of the image size from the original electron beam RMS size is shown in Fig. 10 as a function of the screen thickness and as a function of the beam energy. This difference is the systematic uncertainty in the beam RMS size measurements. The deviation depends on the initial beam RMS size: the less the initial beam RMS size the bigger deviation will be observed. The systematical uncertainty can be increased up to 5 μm for 0.1 mm beam RMS size ($\sim$ 5%) and 2.5 μm for 0.5 mm beam RMS size ($\sim$ 0.5%).

4.3 Comparison of different methods

In the ideal case all methods of the beam profile measurements must give the same results. But in reality they always have some systematical difference in measurements due to the individual features. To compare the different methods two experiments were done: 1) cross check measurements between the YAG screen stations and the wire scanner; 2) comparison of profiles from the YAG and the OTR screens.

Table 6: Main beam parameters during the experiment.

Main beam parameters	
Mean momentum	11.7 MeV/c
Bunch charge	1 nC

4.3.1 Wire scanner and YAG screen stations

There is no simple technical way to place a YAG screen station and a wire scanner at the same position and, thus one can‘t compare these devices directly. Therefore measurements were done at three YAG screen stations (EMSY1, High1.Scr3 and High1.Scr5) and the wire scanner between them (Wire scanner 1). Positions of the screen stations and the wire scanner are shown in Fig. 1. The main beam parameters are listed in Table 6. During the experiment all injector parameters were not changed. Transversal beam profiles were measured at three YAG screen stations and the wire scanner.

RMS size calculation can be done either directly for discrete distribution which is our experimental data or after fitting the last one with a well known function. The beam profile is changing while an electron beam passes along the beam line and it can not be described by simple function. Therefore one has to use direct experimental data to calculate a beam RMS

size for the YAG screens and for the wire scanner.

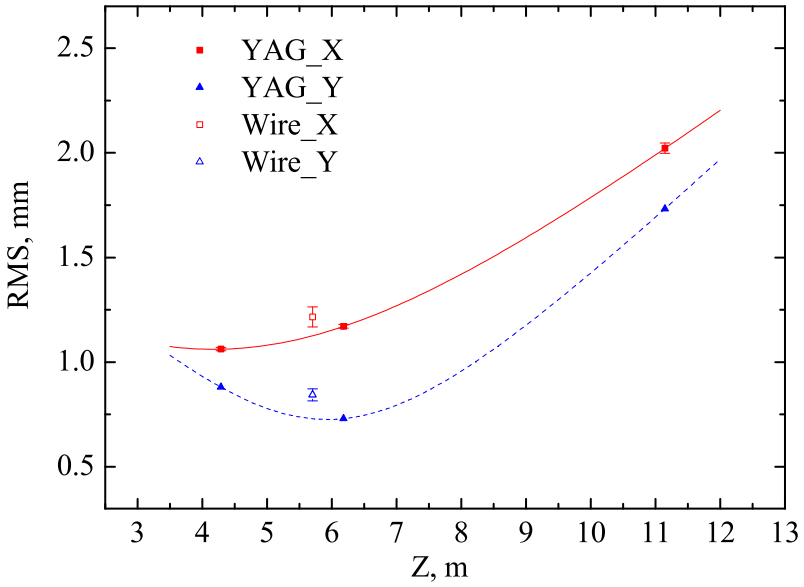

Figure 11: Cross check measurements between the YAG screen stations and the wire scanner. Beam RMS sizes are shown versus Z (the distance from the photocathode).

The RMS size of the electron beam is a function of the distance from the photocathode. The particle behavior in the drift space is known [13]. Therefore the data obtained from the YAG screen stations is fitted by the square root of the second order polynomial equation to find the beam RMS size at the wire scanner position (see Fig. 6). The RMS size measured by the wire scanner was compared with the RMS size value given by the YAG screen stations. The wire scanner gives a larger RMS size value than one measured with the YAG screens. The difference between them is approximately 10% for both X and Y profiles. On the one hand a possible reason is the signal degradation during the transportation from the camera chip to the PC for YAG screen stations (see Section 4.5). On the other hand a wire scanner is sensitive to the beam position fluctuations because it

measures the beam profile during several beam trains. Both the effects can add the systematical uncertainty in the beam size measurements. Other systematical uncertainties for wire scanner measurements should be found. For the next measurements one has to measure beam position fluctuations during the experiment.

4.3.2 YAG and OTR screens

Comparative measurements were done at EMSY1 - the first screen station after the booster section. From both the screens, the YAG and the OTR, the light passes through the same optical system and it is collected by the same camera. In a YAG screen electrons pass the material of some thickness before their energy is transformed into the light. Besides in a YAG screen the light is produced in a finite scintillation layer. An OTR screen does not have such disadvantages. From this point of view an OTR screen must have better resolution than a YAG but an OTR intensity has a big angle spread at low energies ($5 \div 13$ MeV). Therefore the light intensity from the OTR screen collected with our optics is significantly less than from the YAG.

Table 7: Comparison of beam RMS size measurements with YAG and OTR screens.

	YAG screen		**OTR screen**	
Series	x RMS, mm	y RMS, mm	x RMS, mm	y RMS, mm
1	1.250±0.01	1.207±0.008	1.127±0.003	1.082±0.003
2	0.865±0.013	0.718±0.015	0.815±0.013	0.577±0.014
3	0.899±0.005	0.690±0.02	0.860±0.01	0.590±0.003

The main electron beam parameters during the experiment are listed in Table 6. The OTR screen at the current electron energy at PITZ has by factor of eight less light output than the YAG screen. Therefore one

had to increase the number of the laser pulses for the measurements at the OTR screen to have approximately the same output light intensity from both the screens, the YAG and the OTR. Data from three series of the experimental measurements are summarized in Table 7. All experiments were done at the same screen station. Difference between the beam RMS size values measured with the YAG and the OTR screens is calculated as $100\% \cdot (\sigma_{YAG} - \sigma_{OTR})/\sigma_{YAG}$ and is shown in Fig. 12.

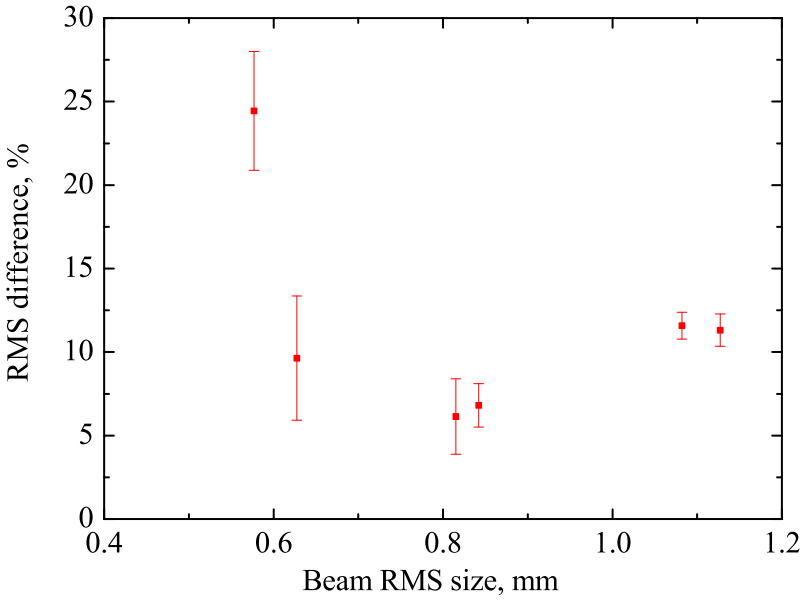

Figure 12: Difference between RMS size measurements with the YAG and OTR screens.

The difference amounts to 140 μm and does not show any regularity as a function of the beam RMS size. As expected the YAG screen gives higher values for beam RMS size than the OTR screen due to the multiple scattering effect (see Section 4.2). But the values of the difference are several times more than that, predicted from the multiple scattering effect. The reason could be the optical effects such as the depth of focus issues and the light reflected from the back surface of the scintillator material.

Optical effects increase the measured beam size but it seems that such a big discrepancy can not be explained only by the optical effects in the YAG [19]. Possible explanation is that there was some shift in timing between the gun and the booster RF pulses, so that the head of the train was accelerated only in the gun and has the energy of 5 MeV. It is not possible to check the timing history. One has to repeat these measurements for different positions along the beam line at PITZ.

4.4 Stability of photo injector parameters

Beam dynamics is sensitive to a lot of injector parameters. Two of the main parameters are the bunch charge and the mean electron beam energy. The bunch charge depends on the laser intensity, on the RF phase and the peak field in the gun and on the quantum efficiency of the photocathode. The mean beam energy depends mostly on the gun power. A beam RMS size is a function of the beam energy mainly because of the solenoid focusing. Besides, it depends on the bunch charge because of the space charge forces. Thus, a variation of the beam parameters can change beam dynamics that influences the uncertainty in the beam RMS size measurements. Simulations of the beam dynamics were done to find the dependence of the beam RMS size variation as a function of the charge and the energy fluctuations. ASTRA tracking algorithm was used for the simulations. All simulation settings were close to the experimental values during the emittance measurements.

Injector stability can influence the statistical uncertainty as well as the systematical uncertainty. If we collect the light from a screen during one train (usual screen station operation) a beam position jitter inside the train systematically increase the beam size under measurement. Beam position

jitter can be induced either by laser position jitter [33] or by instability of power supply of steering magnets. A position jitter between the trains brings to the statistical uncertainty for the screen stations, but for the wire scanner it brings systematical uncertainty. Thus, we have to distinguish between the short time term stability (during one train) and the long time term stability (during several trains).

4.4.1 Bunch charge stability

ASTRA simulations were done for five different initial charges (Fig. 13 (left)). The difference in the beam RMS size depends on the distance from the cathode Z and it can be represented as a linear function of the bunch charge at a given position Z for small charge fluctuations. The difference

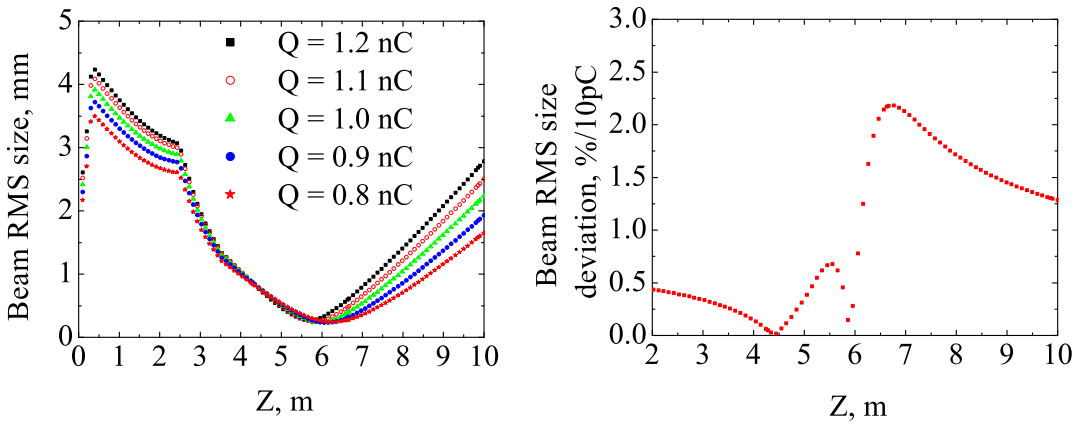

Figure 13: Beam RMS size as a function of the distance from the cathode (left). Beam RMS size deviation in percent per 10 pC charge fluctuation for 1 nC electron beam charge (right).

amount to the 2.2% of the beam RMS size deviation per 1% of charge fluctuation at the 1 nC bunch charge (Fig. 13 (right)). The sensitivity to the charge fluctuations is lower before the beam focusing point and reaches

the maximum value after it.

Charge jitter at the same number of the laser pulses for PITZ setup is about 2% hence using ASTRA simulation results we obtain the maximum beam RMS size jitter of 4.4%. The experimental value of the statistical uncertainties in the beam RMS size measurements is about 2% (see Table 7). It is two times less than the maximum value obtained from the ASTRA simulations (4.4%). The charge stability from pulse to pulse has not been studied systematically yet.

4.4.2 Electron beam energy stability

Beam energy E depends linearly on the maximum electric field in the cavity at the constant RF phase and therefore it depends as a square root on the power P absorbed in the gun [13]

$$E = e \cdot \sqrt{r_s L P}\sqrt{1 - e^{-2\tau}}\cos\varphi_s, \tag{33}$$

where e is the electron charge, r_s is the shunt impedance per unit of length, L is the length of the cavity, τ is the attenuation factor and φ_s is the synchronous phase. After the variation of the Eq. (33) and dividing the result by the same equation to exclude the unknown coefficients we obtain the uncertainty relationship:

$$\frac{\delta P}{P} = 2\frac{\delta E}{E} \tag{34}$$

For the usual operating regime at PITZ, the power in the gun is $P = 3.3$ MW and the beam energy after the gun is $E = 4.5$ MeV, thus Eq. (34) gives:

$$\delta P[kW] = 1.5 \cdot \delta E[keV] \tag{35}$$

Fig. 14 (right) shows the results of the simulation for six different maximum electric fields in the gun and for 1 nC beam charge. The beam RMS

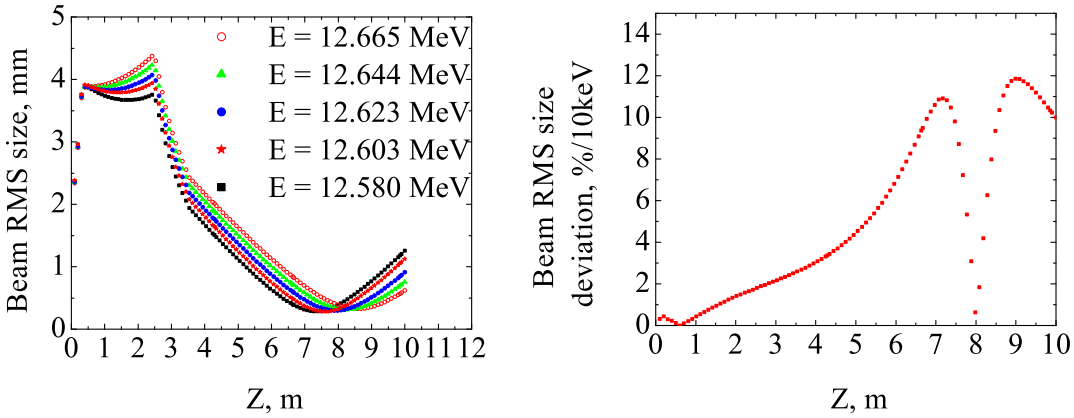

Figure 14: Beam RMS size as a function of the distance from the cathode (left). Beam RMS size deviation in percent per 10 keV mean energy fluctuation for 1 nC electron bunch charge (right).

size sensitivity to the energy fluctuation is shown in Fig. 14 (left). The maximum uncertainty in the beam RMS size is about 10% per 10 keV in the electron beam energy fluctuation. During the usual operation regime the gun absorption power has a 7 kW jitter and about 0.4 kW/μs slope along the pulse length. The 7 kW power jitter should lead to the 5 keV of the mean energy fluctuations (Eq. (35)) that corresponds to the energy measurements in LEDA [32]. The 5 keV energy jitter must lead to the 5% maximum statistical uncertainty in the beam RMS size measurements that is close to a measurable value of 2%. The beam RMS size from pulse to pulse has not been studied systematically yet.

4.5 Camera and signal transportation setups

One of the most important steps in beam RMS size measurement is registration of the light from the screen with a camera, image acquisition and further transmission to a PC. The main important characteristics are

the camera's noise level and the bit-depth of ADC. The noise level of a camera depends mainly on camera type and was not considered in this work.

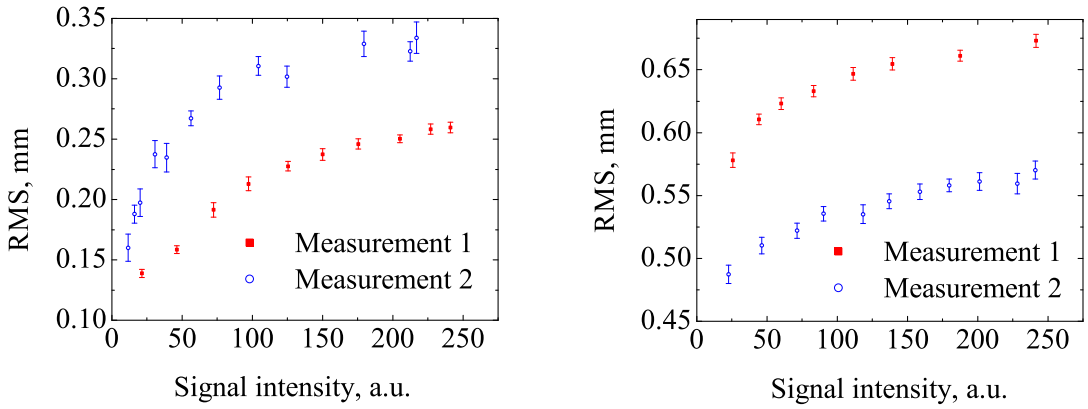

Figure 15: Beam (left) and beamlet (right) size degradation. RMS size is shown as a function of the input signal intensity into the ADC. In the graph a signal intensity means the intensity of the brightest pixel in the distribution. Two examples are shown in both the graphs.

The frame grabber card [34], used at PITZ, is equipped with an 8-bit ADC. An important characteristic of the camera setups at PITZ is a long analog cable line between the camera and the ADC. In this section the signal intensity directly before the ADC will be discussed. The signal intensity level will be expressed in units of the ADC digitalizing step. For an 8-bit ADC, analog signal can be divided in up to 256 ADC steps. One can adjust the signal intensity by changing the number of laser pulses or by adjusting the camera gain. The first option leads to the increasing of the light output from the YAG or the OTR screen. The second one changes the signal amplification after the CCD chip. Both the options give the same result in case they do not change the electron beam profile itself (adjusting the number of the laser pulses) or the image of the electron beam profile

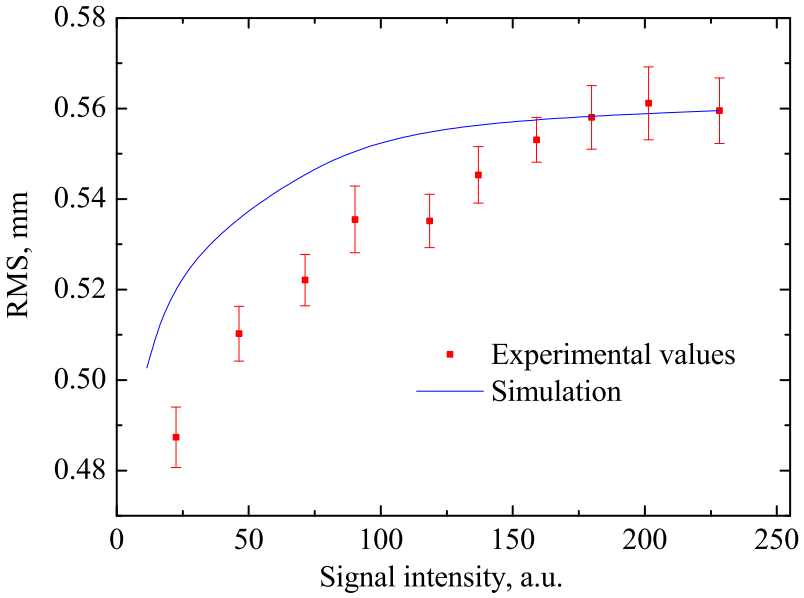

Figure 16: Experimental and simulation results of beam size degradation for the same initial distribution. RMS size is shown as a function of the input signal intensity into the ADC. In the graph a signal intensity means the intensity of the brightest pixel in the distribution.

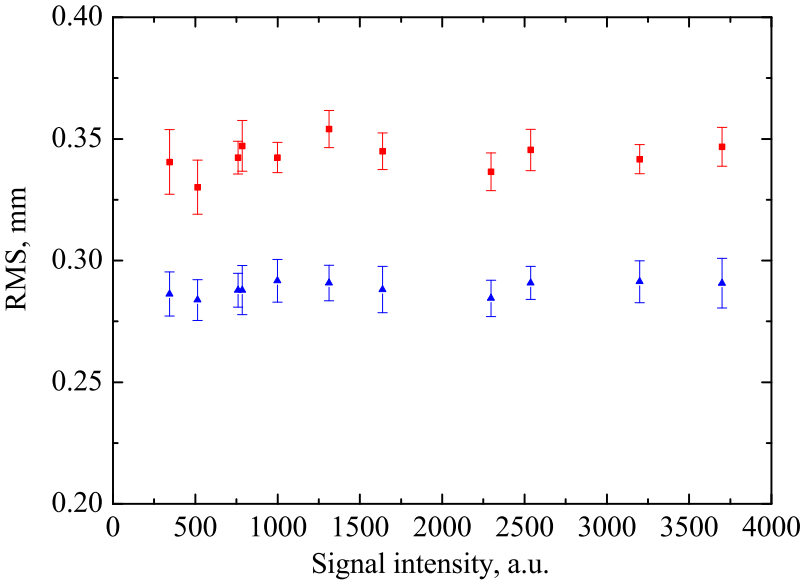

Figure 17: 12-bit camera test. In the graph a signal intensity means the intensity of the brightest pixel in the distribution.

(adjusting camera gain). The first option is not considered here because it can make changes to the beam profile which does not correspond to the signal registration system at all (see Section 4.4). Only the camera gain was used to adjust the signal intensity.

The digitalization process decreases the beam RMS size value because of the cutting of the low intensity edge of the beam image distribution. The beam RMS size uncertainty due to this effect depends on the electron beam profile. An experimental study was conducted to check the influence of the effect. Fig. 15 shows the experimental results for the beam and the beamlet profile measurements. As shown in Fig. 15 by decreasing the signal intensity by a factor of ten comparing to the maximum available value of 255 one can have additional systematical uncertainty up to 20% in the beam RMS size and up to 60% in the beamlet RMS size measurements. This experiment can be compared with numerical calculations. For comparison, the experimental beam distribution at the maximum signal intensity was chosen as an initial distribution. This data was decreased by intensity and after that, values lower than the first ADC level were set to zero. The results were compared to the live data by the PITZ TV system as shown in Fig. 16. A reasonable explanation is the analog signal attenuation during the transport through a long signal cable that connected the camera to the frame grabber.

In addition another camera type was tested at PITZ for future use [35]. It has a 12-bit ADC which is located inside the camera housing. Therefore there is no long analog line. The results of the 12-bit camera tests are shown in Fig. 17. For 12-bit camera there is no visible dependence of the RMS size on the signal intensity as for the cameras used at PITZ.

4.6 Systematical uncertainty of a screen station

Here an example of the systematical uncertainty calculation for the YAG screen station is shown. Let the mean beam energy be 13 MeV and the size of the camera pixels in the object plane be 40 μm. Three types of uncertainties were considered in this work. The first uncertainty is the increasing beam size due to the multiple scattering of electrons in the YAG screen. This uncertainty depends only on the initial beam RMS size if the screen thickness is defined. From Fig. 10 (right) we know the image distribution from the point source. Using Eq. (21) and Eq. (23) one can calculate the beam RMS size uncertainty as a function of the initial RMS size. The second uncertainty is determined by optical resolution. One can estimate this uncertainty by means of Fig. 6. The third uncertainty depends on the pixel size of the CCD chip. This uncertainty is shown in Fig. 8. The values of the three systematical uncertainties and their sum

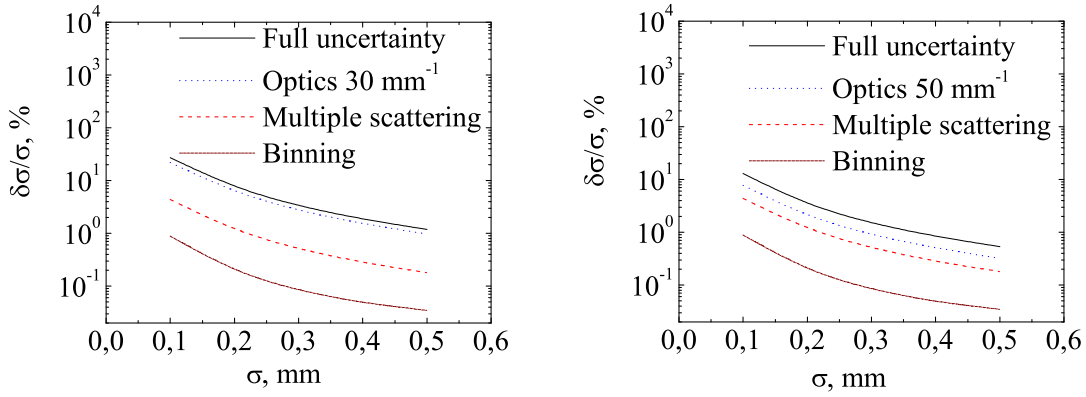

Figure 18: Three components of the systematic uncertainty and their sum for 30 mm^{-1} (left) and 50 mm^{-1} (right) optical resolution.

are shown in Fig. 18 for 30 mm^{-1} and 50 mm^{-1} optical resolution. The uncertainty due to the limit optical resolution is predominant for both the

cases but for 50 mm^{-1} optical resolution it becomes close to the uncertainty caused by the multiple scattering.

Three very important uncertainties are not included: the increase of beam size due to the defocusing effect, image attenuation during the signal transportation to the ADC and the cutting of the low intensive edge of the image in the ADC. The second one can significantly decrease the measured beam size.

4.7 Summary

The wire scanner and YAG screens give close results with a 10% difference (see Fig. 11). The cross check measurements should be continued with parallel measurements of the beam position jitter to exclude possible systematic uncertainties. The beam parameters are stable enough to keep statistical uncertainty of the beam size measurements in order of 5%. If it is possible, the beam size behavior from pulse to pulse should be studied to have an idea of the beam parameters jitter inside the beam train and its influence on the uncertainty for the beam size measurements. The saturation parameter of the YAG screen was not found due to the small effect and lack of measurement precision. Both the screen types, YAG and OTR should be installed after the quadrupole triplet to have a possibility to use the comparison method of the saturation parameter determination. Two guidelines appeared according to the camera system study: the ADC should be as close as possible to the CCD chip to avoid analog signal attenuation, a 12-bit ADC increases precision of the measurements in comparison with the 8-bit ADC because it can detect signals with lower intensity.

5 Conclusions

Three types of beam profile monitors were considered in this work: a YAG screen station, an OTR screen station and a wire scanner. A YAG screen has better sensitivity to the low energetic beam (5÷13 MeV) than other monitors therefore it is most widely used at PITZ at the moment. On the other hand an OTR screen has a better resolution and can be widely used in the future at higher beam energies at PITZ2. For a 13 MeV electron beam OTR screen has eight times less light output than YAG. The disadvantage of a wire scanner is the low speed of measurements in comparison with the screen methods. Therefore wire scanner can not be used for beam profile monitoring. A beam position jitter adds some systematical uncertainty in beam size measurements.

The optical resolution depends on magnification. One should use higher magnification in order to have better optical resolution but the light intensity per pixel will be decreased in this case.

Camera setup and signal transmission system are one of the most important part of screen stations. They detect the light from the screen, digitalizes it and sends to a PC. Investigations of the camera setups at PITZ lead to the next conclusions: it would be better to keep an ADC as close as possible to the CCD chip because of the analog signal attenuation. 12-bit ADC instead of 8-bit is more preferable. The own noise level of the cameras should be systematically investigated to have an idea about cameras resolution.

Comparison study between the YAG and OTR screens should be repeated on several screen stations in the high section at PITZ. Cross check measurements between wire scanners and screen stations should be contin-

ued to find the reason for the systematical difference between their measurements.

The systematical uncertainty for a YAG screen station can reach up to 20% at low beam sizes. Section 4.6 shows an example of the systematical uncertainty calculation. The uncertainty due to the signal attenuation and analog to digital conversion is not included.

References

[1] W. Ackermann et al., Operation of a Free Electron Laser in the Wavelength Range from the Extreme Ultraviolet to the Water Window, submitted to Science.

[2] The Electron Beam Requirements of the European XFEL, `http://xfel.desy.de/`.

[3] F. Stephan, et al., Recent results and perspectives of the low emittance photo injector at PITZ, in Proceedings of the FEL 2000, Italy, Trieste, August (2004).

[4] Thomas Wangler, Principles of RF linear accelerators, chapter 9, pp. 261-264, John Wiley & Sons, USA, (1998).

[5] K. Floetmann, A Space Charge Tracking Algorithm (ASTRA), `http://www.desy.de/~mpyflo/`, December (2006).

[6] Geometry and Tracking (GEANT4) Platform for the Simulation of the Passage of Particles through Matter, `http://geant4.web.cern.ch/geant4/`, December (2006).

[7] J. Baehr et al., Upgrades of the Laser Beam-Line at PITZ, in Proceedings of FEL 2005, Stanford, USA, August (2005).

[8] J. Han, Dynamics of Electron Beam and Dark Current in Photocathode RF Guns Ph.D. thesis, Hamburg University, (2005).

[9] Alexander Wu Chao and Maury Tigner, Handbook of Accelerator Physics and Engineering, 2nd edition, World Scientific, USA, (1998).

[10] L. Staykov, I. Tsakov, Design Optimization of an Emittance Measurement System at PITZ, DIPAC'05, Lyon, France, June (2005).

[11] H.-J. Grabosch, M. Sachwitz, Test of Wire-Scanner at PITZ I, PITZ Note 574, (2003).

[12] K. Floettmann, D. Lipka, Principle of Momentum and Momentum Spread Measurement at PITZ, PITZ Note 05-02, December (2002).

[13] Helmut Wiedemann, Particle Accelerator Physics, vol. 2, chapter 5, pp. 162-164, chapter 2, pp. 38-42, Berliner Springer, Berlin, 2nd edition, (2003).

[14] L. Staykov et al., Commissioning of a New Emittance Measurement System at PITZ, FEL06, Berlin, Germany, August (2006).

[15] L. Staykov, Transverse Electron Beam Phase Space Characterization at PITZ using Preliminary Booster, Ph.D. thesis, Hamburg University (to be published).

[16] G. Asova, Phase Space Tomography Diagnostic at the PITZ Facility, in Proceedings of ICAP 2006, Chamonix, France, October (2006).

[17] Data base of the National Institute of Standards and Technology, `http://www.physics.nist.gov/`, December (2006).

[18] Shihong Zhou et al., Spectral Properties of Rare-Earth Ions in Nanocrystalline YAG:Re (Re = Ce^{3+}, Pr^{3+}, Tb^{3+}), J. Lumin. 118, 179 (2006).

[19] A. Murokh, et al., Limitations on the Resolution of YAG:Ce Beam Profile Monitor for High Brightness Electron Beam, 2nd ICFA Ad-

vanced Accelerator Workshop on the Physics of High Brightness Beams, Los Angeles, USA, November (1999).

[20] D. Lipka Saturation of Light Intensity from a YAG-screen at the TESLA Test Facility, PITZ Note 09-01, (2001).

[21] T. Ludziejewski et al., Investigation of Some Scintillation Properties of YAG:Ce crystals, Nucl. Instr. and Meth. A398, 287 (1997).

[22] C. Yang, Radiation of Fast Charged Particles in Media, Chinese journal of physics, vol. 30, No 3, June (1992).

[23] E. Bravin and T. Lefevre Studies of OTR Angular Distribution on CTF2, in Proceedings DIPAC 2003, Mainz, Germany, May (2003).

[24] M.-A. Tordeux, J. Papadacci A New OTR Based Emittance Monitor for the Linac of LURE, in Proceedings of EPAC 2000, Vienna, Austria, June (2000).

[25] N. V. Bargen et al., Wire Scanner for the Undulator Section of the Free Electron Laser at the Tesla Test Facility - Phase II, HASYLAB, Annual report, (2003).

[26] T. Okugi et al., Evaluation of Extremely Small Horizontal Emittance, Phys. Rev. ST AB 2, 022801 (1999).

[27] Optical System Specification for the "Optem" Lens, `http://www.qioptiqimaging.com/Products/MachineVisionLenses/MVZLMacroVideoZoomLens/`, December (2006).

[28] Bingxin Yang, Optical System Design for High-Energy Particle Beam Diagnostics, Beam and Instrumentation Workshop Uptown, New

York, May 6-9, 2002 AIP Conference Proceedings Vol. 648 pp. 59-78 (2002).

[29] CV-M10SX Monochrome Progressive Scan Camera, Operation manual, http://www.jai.com/camera/products_info.asp/id=312&sprog=uk.

[30] SONY ICX415AL CCD Chip Data Sheet, http://www.framos.de/www.dir/ru/produkte/ccdsensoren/image/prog_scan_sys/prod.dir/1862/index_ru.html, December (2006).

[31] Claus Grupen, Cambridge Monographs on Particle Physics, Nuclear Physics and Cosmology, vol. 5, Particle Detectors, chapter 1, pp. 17-20 Cambridge University Press, (1996).

[32] L. Staykov, PITZ logbook, DESY, Zeuthen, October (2006).

[33] Ye. Ivanisenko, Photoinjector Laser Beam Intensity and Position Monitoring System, Diploma thesis, Karazin Kharkiv National University, (2007).

[34] Frame Grabber card, http://www.coreco.com/Web/download.nsf/AllDocsById/E22011658E96679385256A380076426B/\$File/PCVision.pdf, December (2006).

[35] Prosilica GE 1350, http://www.prosilica.com/, December (2006).

Acknowledgements

I would like to thank many people for contributing to the Happy End of my diploma thesis. First of all I want to express my gratitude to my supervisors Lazar Staykov and Sergiy Khodyachykh for their continuous support of my work. They gave me a lot of pieces of helpful advice during my work and carefully read my manuscript. My special thanks are addressed to Frank Stefan for giving this great opportunity to work at PITZ facility. I thank to Hans-Juergen Grabosch for providing documentations for wire scanners. The experimental results would not have been possible without the people from PITZ group, who participated in the shift operations: G. Asova, J. Bahr, L. Hakobyan, Ye. Ivanisenko, H.-J. Grabosch, S. Khodyachykh, S. Korepanov, M. Krasilnikov, A. Oppelt, B. Petrosyan, J. Roensch, L. Staykov, F. Stephan, S. Weisse. I thank Juergen Baehr, Mikhail Krasilnikov and Stefan Weisse for the numerous helpful discussions which have helped me better to understand the problems and find solutions to them. For the software support I also wish to acknowledge Galina Asova.

I am very grateful to Dr. E. Shmatko and Dr. V. Afanasev for giving great education.

Finally, I wish to thank my family for their warm encouragement during my staying in Germany.